JOURNAL OF MATERIALS SCIENCE 16 (1981) 2145–2153

The physical and structural properties of superconducting A15-type Nb–Sn alloys

H. DEVANTAY, J. L. JORDA, M. DECROUX, J. MULLER
Département de Physique de la Matière Condensée, Université de Genève, 1211 Genève 4, Switzerland

R. FLÜKIGER
Kernforschungszentrum Karlsruhe, Institut für Technische Physik, Postfach 3640, 7500 Karlsruhe, West Germany

Bulk samples covering the entire homogeneity range of the Nb–Sn A15-phase were prepared by a new method: levitation melting under high argon pressure. The variations of the lattice parameter, superconducting transition temperature, resistivity and critical field slope were measured as a function of composition. A low-temperature X-ray diffraction study was undertaken in order to fix the compositional limit of the tetragonal phase. The theoretical expectations for the critical field slopes at the transition temperature, T_c, based on actually-observed alloy parameters, were found to be in good agreeement with measured values.

1. Introduction

The extraordinary interest shown in Nb_3Sn arises from the fact that this compound is one of the most attractive materials for the construction of high-field superconducting magnets [1]. Moreover, Nb_3Sn has been widely used for testing various theoretical models dealing with electronic properties of high-field superconductors particularly in the case of the prominent A15-type phases [2]. However, in spite of several hundreds of publications on Nb_3Sn, a number of questions remained unanswered concerning the variation of basic physical properties as a function of composition, $Nb_{1-\beta}Sn_\beta$, where β is the Sn concentration, and to some extent also the changes of these properties with the martensitic transformation. The reason for this is connected with the great difficulties encountered in preparing well-characterized, homogeneous samples over the whole homogeneity range of the A15-type Nb_3Sn phase, $0.18 \leqslant \beta \leqslant 0.25$.

A brief review of the literature shows that even the variation of the lattice parameter as a function of Sn content shows different trends, depending on whether data is obtained on bulk samples [3, 4] or on samples prepared by chemical vapour deposition (CVD) [5]. The relation between the transition temperature, T_c, and β was found to be fairly linear in an investigation on a series of vapour-deposited films [6, 7] while a large dispersion was reported in other studies on thin film samples [5] and bulk samples [4]. Our own previous investigations [8] have further indicated that it is not possible to produce homogeneous specimens of *intermediate* composition ($\beta < 0.25$) by sintering reactions, a technique which is otherwise successful for producing the stoichiometric compound.

The martensitic transformation of Nb_3Sn was first observed by Mailfert *et al.* [9]. Later, evidence of a first-order transformation was found by Vieland *et al.* [10]. X-ray techniques have been used to study the transformation by King *et al.* [11] and Vieland [12]. Recently, it was found by Flükiger [13] that stresses in multifilamentary wires could induce a cubic-to-tetragonal phase transition in Nb_3Sn-based material.

Numerous upper critical field, $H_{c2}(T)$, measurements for Nb_3Sn have been reported in the literature (for representative data see [14–19]). The recent study of Orlando *et al.* [19] on thin films grown under varying deposition conditions pro-

0022–2461/81/082145–09$02.90/0

vided valuable information on the influence of the residual resistivity on $H_{c2}(T)$. However, no low-temperature structural investigations were undertaken in this work. No measurements at all have been made so far on a series of bulk specimens covering the homogeneity range and combining observations of H_{c2}, the resistivity and the electronic specific heat.

The aim of the present investigation was to establish the variation of some important parameters as a function of composition on a series of bulk alloys prepared by a new method, i.e. levitation melting under high argon pressure, followed by homogenization annealing at a temperature of 1800° C. The initial slope of the critical field and the electrical resistivity of well-characterized samples were measured and are compared with theoretical expectations, using previous specific heat results. Further, the near-stoichiometric specimens were used to determine the homogeneity range of the low-temperature tetragonal phase.

2. Preparation and analysis

The series of alloys $Nb_{1-\beta}Sn_{\beta}$ was prepared from powders of Nb (99.95% purity, obtained from Johnson–Matthey) and Sn (99.9% purity, obtained from Fluka). The mixed powders were compacted, placed in evacuated quartz tubes and heated in stages up to 1050° C over a time of 24 h. The sintered samples were then melted in a levitation coil under an argon pressure of 40 atm. In order to achieve the best possible homogeneity, the ingots were given a high-temperature heat treatment under pressure (1800° C for 12 h for samples near the Sn-rich limit and 1850° C for 27 h for $\beta < 22$ at% Sn). Finally, all the alloys were subjected to a prolonged annealing (3 weeks) in quartz tubes at 1000° C. The microstructure of the samples was investigated using optical microscopy after a chemical etch in a solution of 62 vol% H_2O, 8 vol% HNO_3, 15 vol% H_2SO_4 and 15 vol% HF. X-ray powder diffraction analysis was carried out in a Guinier camera using Cu$K\alpha$ radiation. A low-temperature powder diffractometer, coupled with a helium flow cryostat, was used to measure the high angle Cu$K\alpha_1$/$K\alpha_2$ diffraction lines at a temperature of 10 K.

The superconducting transition temperature was measured inductively on parts of the samples powdered to a size smaller than 38 μm, in order to minimize shielding due to inhomogeneities. The results were satisfactory, but, from previous studies on non-stoichiometric A15-type superconductors, it was born in mind that even by conducting measurements on powders shielding effects are not completely removed, the inductive T_c-values being always somewhat higher than those determined by calorimetric methods. The normal electrical resistivity was measured in a four-point configuration on small bars of dimensions 1 mm × 1 mm × 10 mm, prepared by spark erosion. The contacts were made by silver painting and the temperature was measured with germistor and Pt resistance thermometers. The absolute error in the resistivity is estimated to be less than ± 5%, this error resulting mainly from errors in the measurement of the specimen geometry.

TABLE I Results of concentration analysis

Nominal composition	Calculated composition	Chemical analysis	Microprobe analysis
$Nb_{74}Sn_{26}$	$Nb_{76}Sn_{24}$	$Nb_{75.6}Sn_{24.4}$	$Nb_{75.7}Sn_{24.3}$
$Nb_{75}Sn_{25}$	$Nb_{76.8}Sn_{23.2}$	$Nb_{76.1}Sn_{23.9}$	—
$Nb_{76}Sn_{24}$	$Nb_{77.2}Sn_{22.8}$	—	—
$Nb_{77}Sn_{23}$	$Nb_{78}Sn_{22}$	—	—
$Nb_{78}Sn_{22}$	$Nb_{79}Sn_{21}$	$Nb_{79.6}Sn_{20.4}$	$Nb_{78}Sn_{22}$
$Nb_{80}Sn_{20}$	$Nb_{81}Sn_{19}$	$Nb_{80.4}Sn_{19.6}$	$Nb_{80.3}Sn_{19.7}$
$Nb_{82}Sn_{18}$	$Nb_{83.7}Sn_{16.3}$	—	$Nb_{81.6}Sn_{18.4}$
$Nb_{83}Sn_{17}$	$Nb_{84.5}Sn_{15.5}$	$Nb_{84}Sn_{16}$	$Nb_{82.3}Sn_{17.7}$

Concentration determinations were based on weight control, chemical analysis and microprobe investigation, the latter using the $L\alpha$ lines and the Colby–Niedermeyer correction scheme [20]. The main results are summarized in Table I, where, for the calculated composition, it is assumed that only Sn is lost by evaporation. It is felt that for single-phase samples, the accuracy of the chemical analysis will be slightly better than that of the microprobe analysis.

3. Results

3.1. Phase diagram and lattice parameters

By means of levitation thermal analysis [21], the peritectic formation of the Nb–Sn A15-phase was found, for the temperature 2110 ± 20° C, to be in agreement with the diagram given by Charlesworth *et al.* [22]. At low temperatures (~ 1000° C), the results for the present alloy series confirm the equilibrium phase limits $0.18 \leqslant \beta \leqslant 0.25$ as previously accepted [22], and the results are in essential agreement with the recent microprobe study of Feschotte *et al.* [23]. The combined X-ray and micrographic results obtained by us suggest that the most probable Nb-rich limit should be placed

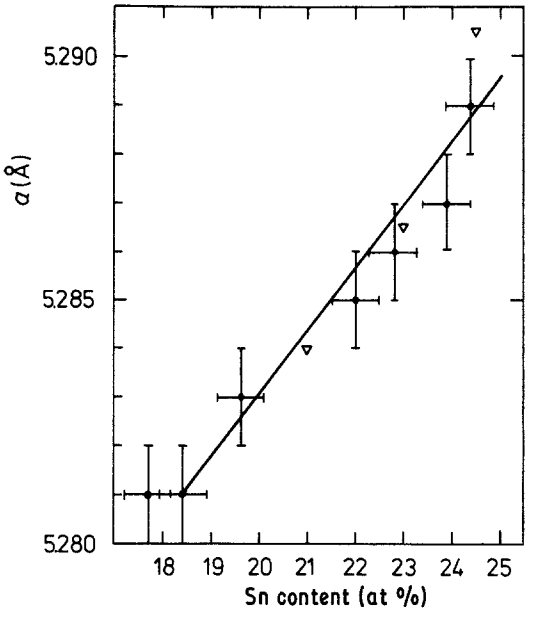

Figure 1 Variation of the lattice parameter, a, within the homogeneity range of the Nb–Sn A15-phase. The data marked ▽ are from Vieland [3].

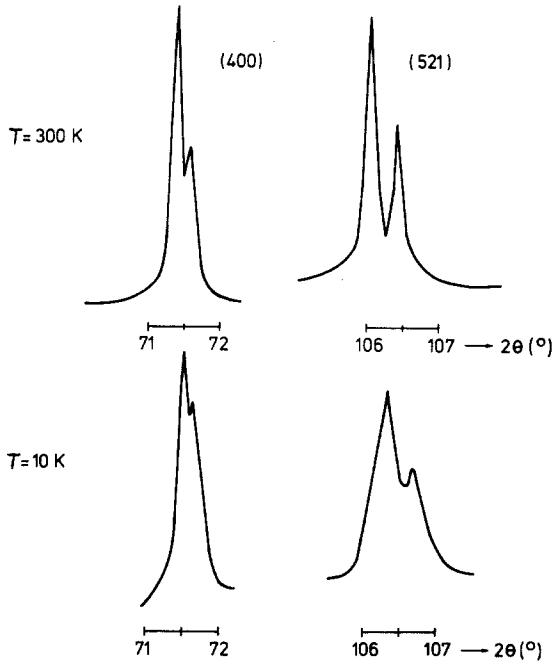

Figure 3 X-ray diffraction peak intensities at 300 K and 10 K for the powdered $Nb_{75.6}Sn_{24.4}$ sample. θ is the diffraction angle. In the tetragonal phase $(c/a) - 1 < 0$, therefore, $\frac{1}{3}$ of the intensity is deplaced towards higher angles and $\frac{2}{3}$ towards lower angles.

between 18 and 19 at% Sn. The lattice parameters, a, accurate to within ± 0.001 Å, vary at room temperature from 5.281 Å to 5.290 Å (see Fig. 1). If 18.5 at% Sn is chosen as the lower limit, a linear extrapolation to hypothetical Nb_3Nb ($\beta = 0$) yields $a = 5.25$ Å which compares favourably with the expected value $4^{1/3}a$(Nb, bcc) = 5.24 Å, suggested by the usually similar atomic volumes in the A15 and A2 structures. The Vickers microhardness (for 100 g load) was also measured throughout the homogeneity range of the A15-phase but no significant variation of microhardness with concentration was observed (see Fig. 2). The average value of the microhardness was measured to be 1100 kg mm^{-2}.

3.2. Structural transformation

As shown in Fig. 3, the powdered $Nb_{75.6}Sn_{24.4}$ sample undergoes a partial low-temperature trans-

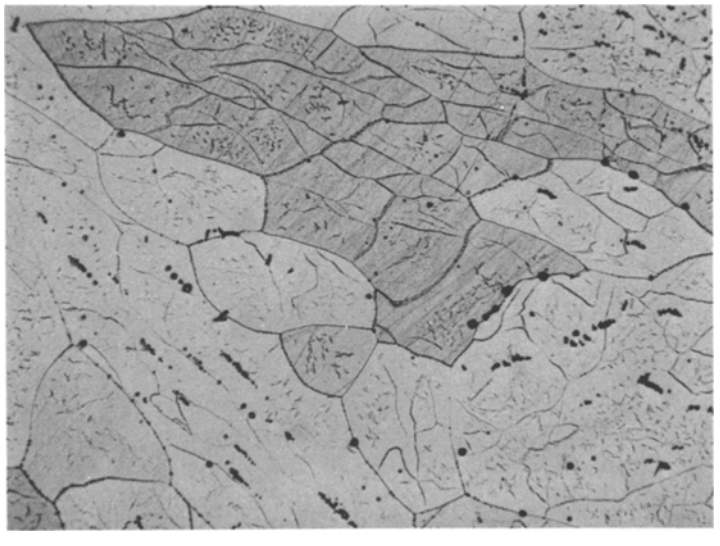

Figure 2 Microstructure of $Nb_{78}Sn_{22}$ after the heat treatment described in the text. Different grain orientations are visible. Microhardness H_V = 1100 kg mm^{-2} (× 150).

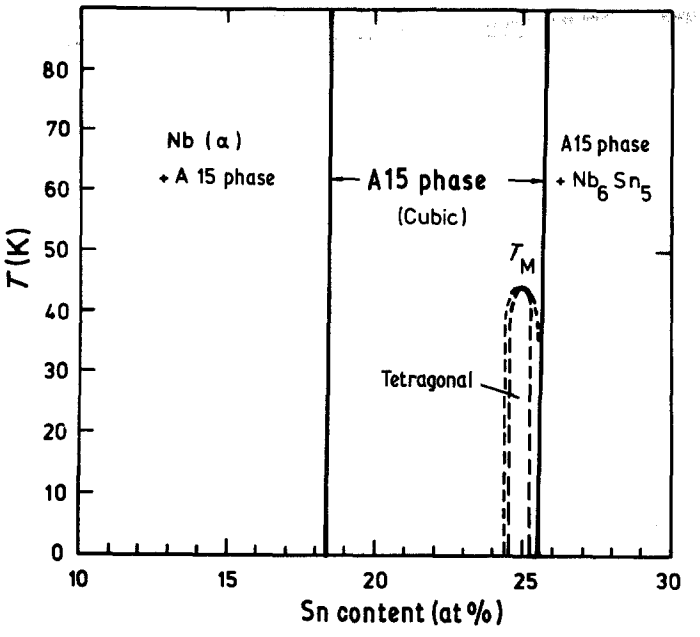

Figure 4 Low-temperature phase diagram. The transformation temperature, T_M, is taken from Mailfert *et al.* [9].

formation. The cubic to tetragonal deformation is evidenced by the shift of the relative intensities of the $K\alpha_1$ and $K\alpha_2$ peaks, in agreement with the known contraction along the c axis $[(c/a) - 1 < 0]$. However, such a shift is no longer detectable at and below a concentration of 24 at% Sn. Taking into account the actual compositional width of these alloys, it was concluded that the limit of the tetragonal phase is near 24.5 at% Sn. Fig. 4 illustrates the most probable narrow range over which the tetragonal structure exists. It should be noted that the possible boundaries of a two-phase region have not the same significance as is usual in phase diagrams, since the microscopic concentration profile is frozen-in. A two-phase range may however exist in an internal stress field.

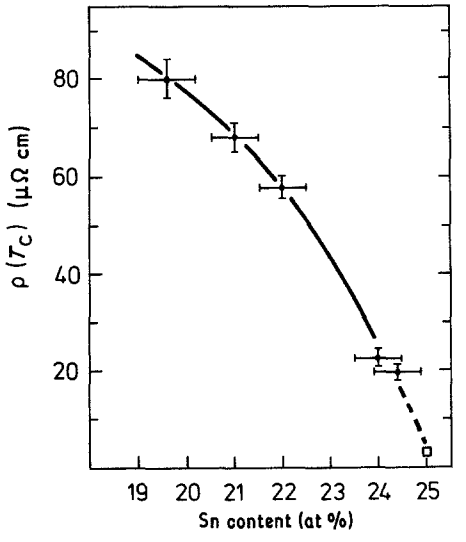

Figure 5 Residual resistivities at T_c of bulk Nb–Sn alloys.

3.3. Resistivities

The specific electrical resistivities, ρ, as measured just above the superconducting transition temperatures, are reported in Fig. 5. It is believed that the values obtained are representative for fairly homogeneous, crack-free alloys of compositions from 19 to 25 at% Sn. The phonon contribution to the electrical resistivity expected for ideal Nb_3Sn at $T_c = 18$ K is estimated to be 3 $\mu\Omega$ cm, as indicated by a quadratic extrapolation to $T = 0$ (insert of Fig. 6).

3.4. Superconducting properties

The inductively-measured transition intervals are reported in Fig. 7. Taking into account the remarks already made on shielding effects resulting from remaining inhomogeneities (see Section 2) and also the uncertainties in absolute concentration, the best conclusion that can be drawn at this stage is that T_c varies linearly between the limits of the phase (Section 3.5 and Fig. 12). The values corresponding to the limits are 6.0 K at 18.5 at% Sn and 18 K at 25 at% Sn (onset 18.2 K for the 24.4 at% sample). An attempt was made to detect variations of T_c with the equilibrium order parameters at fixed composition by taking measurements in the

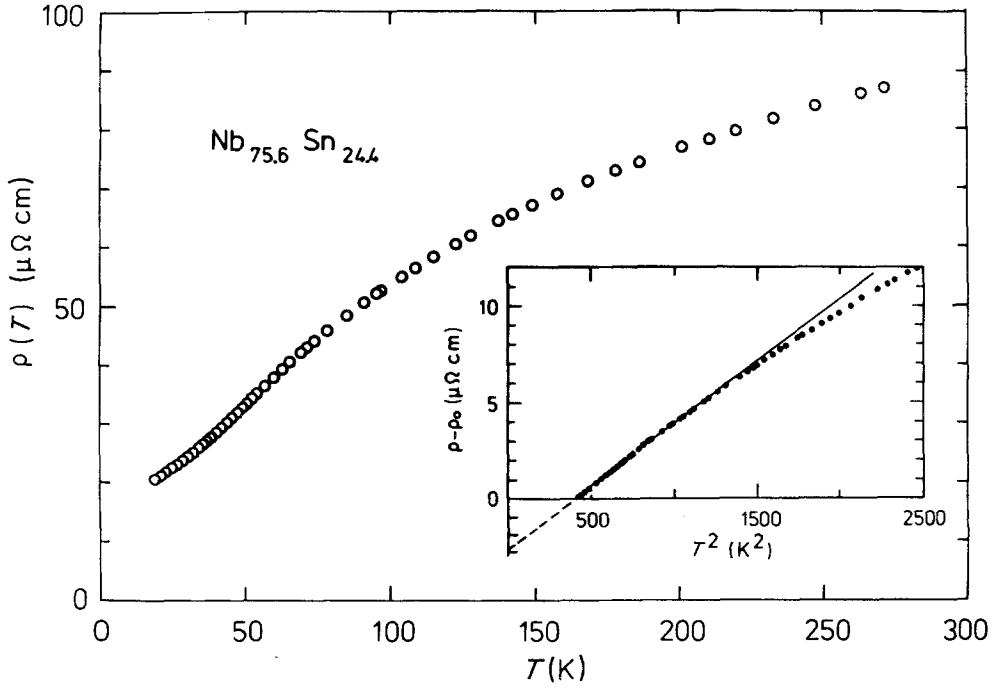

Figure 6 Resistivity, $\rho(T)$, of $Nb_{75.6}Sn_{24.4}$. Quadratic extrapolation in the insert shows the phonon contribution to the resistivity at T_c.

annealed state (1000° C) as well as after argon-jet quenching from 1800° C (cooling rate $\simeq 10^4$° C sec^{-1}). In the two sets of observations, only rather small decreases of the transition temperature in the quenched state could be found, not exceeding 0.5 K. This result is somewhat surprising for the high-T_c specimens but does not necessarily contradict earlier findings in related systems [24]. Two tentative explanations may be given:

(a) the order parameter, S_A, is not decreased substantially at 1800° C, which is 300° C below the peritectic formation temperature (quenching from above 1800° C is not suitable because of the form of the phase diagram);

(b) the retained order parameter does not correspond to its high-temperature equilibrium value for reasons connected with the kinetics of this system.

It appears that Nb_3Sn is a bad choice for studying the effect of thermal disorder on superconductivity.

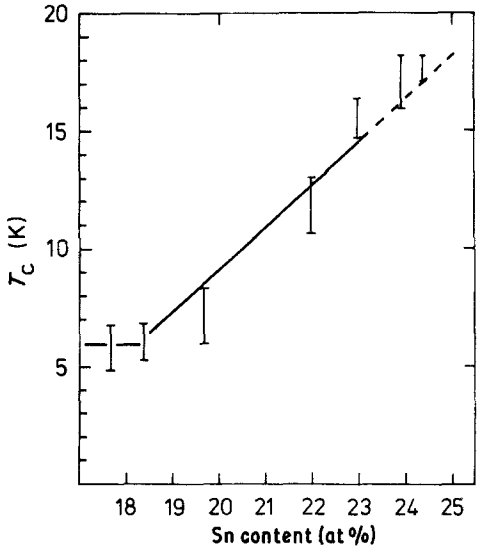

Figure 7 Inductively-measured transitions of melted Nb–Sn alloys.

The results of the resistively-measured upper critical fields, up to 7 T, are reported in Fig. 8 for the two samples with the highest mean Sn concentration. For these bulk alloys, the interesting fact was noticed that H_{c2} against T plots exhibit a distinct positive curvature, most pronounced around 2 to 3 T. The deviation from the Ginzburg–Landau–Abrikosov–Gorkov (GLAG) critical field (linear in this temperature interval) is seen in Fig. 9, using the reduced variables $t = T/T_c$ and $h_{c2} = H_{c2}(T)T_c^{-1}(dH_{c2}/dT)^{-1}_{T_c}$. Such an effect has been observed earlier (see, for example [19]) and has

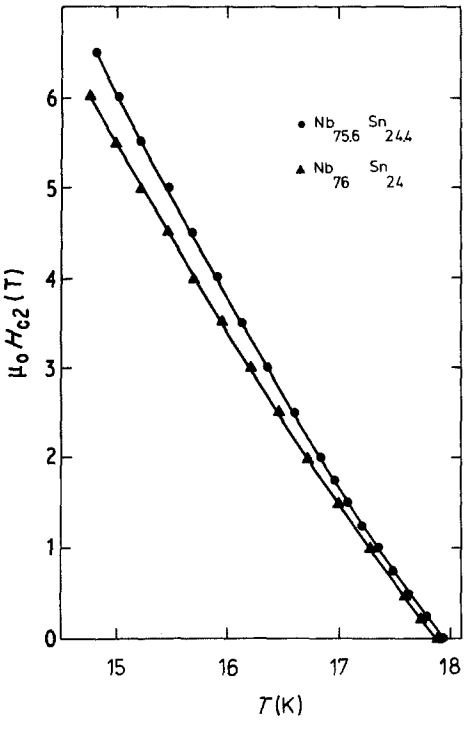

Figure 8 Upper critical fields of near-stoichiometric samples. For $Nb_{75.6}Sn_{24.4}$, the slope $d\mu_0 H_{c2}/dT$ is $1.68\,T\,K^{-1}$ at T_c but $2.55\,T\,K^{-1}$ at 15 K.

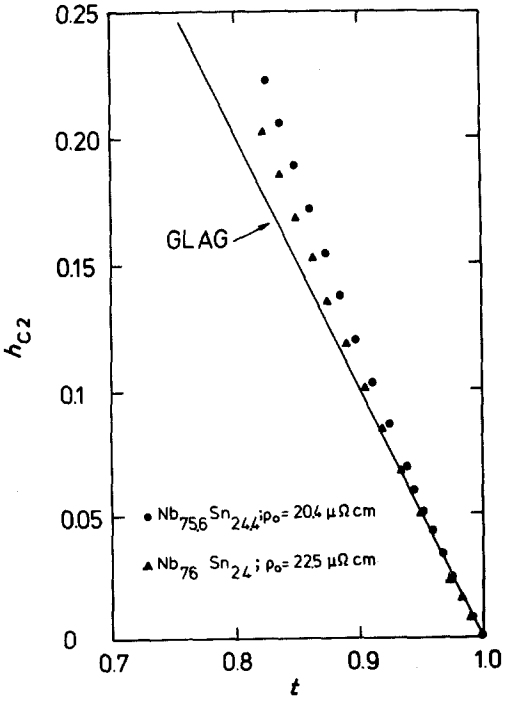

Figure 9 Data of Fig. 8 plotted in reduced variables $h_{c2}(t)$.

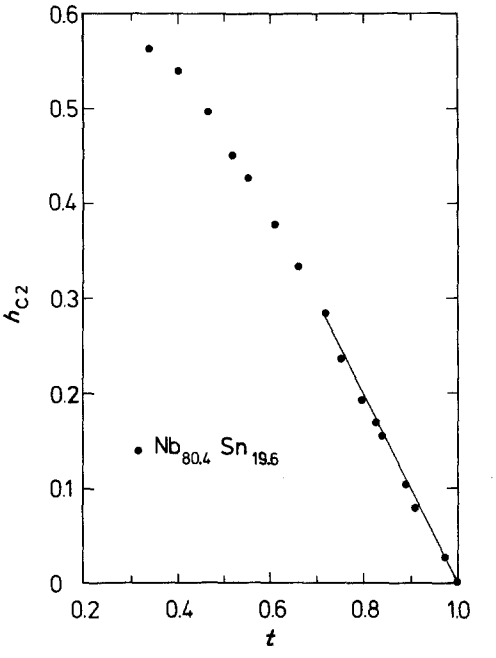

Figure 10 Reduced upper critical field against T plot for $Nb_{80.4}Sn_{19.6}$. The measured slope at T_c is $1.63\,T\,K^{-1}$.

not been given a satisfactory explanation, although it could qualitatively result from anisotropy. This will be discussed in more detail in Section 3.5. As shown in Fig. 10, the critical field against temperature plot of an alloy with strong deviation from stoichiometry shows no positive curvature and is linear down to $t \simeq 0.7$. The positive curvature effect vanishes below 24 at% Sn.

3.5. Analysis of the critical field slopes

To evaluate the expected variation of the upper critical field slope at T_c, the following expression [19] is used:

$$-\left(\frac{\partial \mu_0 H_{c2}}{\partial T}\right)_{T_c} = \left[an^{-4/3}\left(\frac{S}{S_f}\right)^{-2}\gamma_V^2 T_c + b\rho\gamma_V\right] \times \frac{R(\infty)}{R(\lambda_{tr})}\eta_{H_{c2}}(T_c), \quad (1)$$

where a and b are constants with values of $8.1 \times 10^{30}\,K^2\,A^{-1}\,J^{-1}$ and $4.4 \times 10^3\,K^2\,V^{-1}$, respectively, n is the electron density (taken as 2×19 per unit cell for the stoichiometric compound), S/S_f is the ratio of the areas of the Fermi surface to the free electron Fermi surface, $\gamma_V = \gamma/V_{at}$ is the coefficient of the electronic specific heat per unit volume and $\eta_{H_{c2}}(T_c)$ is the

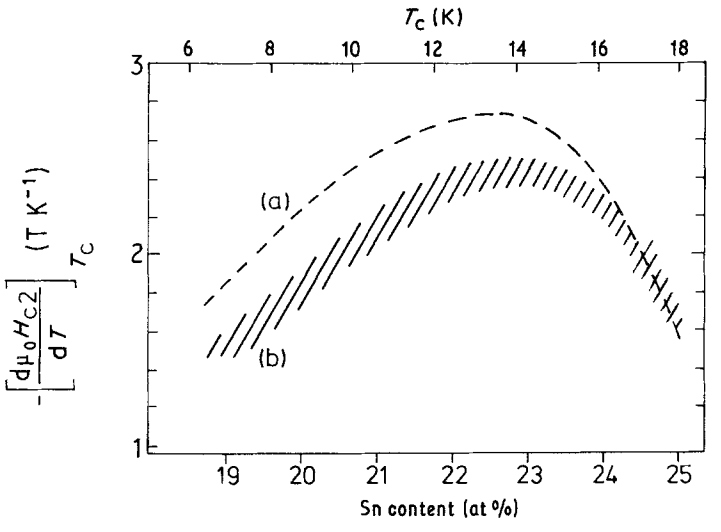

Figure 11 Curve (a) calculated critical field slope of Nb–Sn alloys. Area b: experimental values, taking into account compositional and measurement uncertainties.

strong coupling correction factor. Following the work of Orlando *et al.* [19], we have adopted $S/S_f = 0.35$ (the choice of this value is not critical below about 23 at% Sn). The strong coupling correction factor $\eta_{H_{c2}}(T_c)$ is assumed to increase linearly from unity to 1.17 within the homogeneity range. The factor $R(\infty)/R(\lambda_{tr})$, related to the coherence length and the mean free path, may be taken to be unity over most of the homogeneity range and to be 1.17 for the ideal compound.

The calculated values of $(\partial H_{c2}/\partial T)_{T_c}$ are shown in Curve a in Fig. 11. This curve is based on the resistivity data taken from Fig. 5 and a linear variation of the electronic specific heat coefficient between 5 and 13 mJ K^{-2} per gram atom measured at the Nb-rich boundary and at Nb_3Sn, respectively [25]). Experimentally-observed slopes fall within the hatched area b in Fig. 11, which is very close to the predicted values. It should be noted that for near-stoichiometric compositions, we have retained the tangent strictly at T_c rather than that from the steeper part of $H_{c2}(T)$.

The question of the significance of the observed positive curvature may now be taken up again. Indeed, such a positive curvature could in principle arise from the transition width caused by inhomogeneities. To picture such an effect, one may construct a positively curved $H_{c2}(T)$ plot as the envelope of a family of intersecting straight lines corresponding to a distribution of T_c in the sample. An attempt has been made to analyse the measurements corresponding to the near-stoichiometric specimens in such a way, using best-estimated concentration profiles and a linear variation of T_c with composition, slightly below 25 at% Sn. The result is not satisfactory since it is necessary to invoke a variation of dH_{c2}/dT with concentration significantly steeper than indicated on the corresponding part of Fig. 11. It may be questioned if the positive curvature is an intrinsic property of Nb_3Sn. Fermi surface and pairing anisotropies could produce such effects [26–29], but their occurrence at rather high reduced temperatures, such as observed here, can not easily be understood. Furthermore, Foner and McNiff [17] have established that the anisotropy of the critical field is small in Nb_3Sn.

The approximate coincidence of the cubic to tetragonal phase boundary, which it was possible to locate near 24.5 at% Sn, and the concentration characterized by the critical field anomaly, strongly suggests that the two facts are related. The steeper part of $H_{c2}(T)$ is likely to correspond to the cubic volume fraction with somewhat lower Sn-concentration. The more detailed T_c variation required to explain the measured $H_{c2}(T)$ is reproduced in Fig. 12. Such a slight dependence on structure may be considered a refinement of Fig. 7.

In the case of the 24.4 at% Sn sample, the resistive upper critical field at 4.2 K has been checked in a pulsed field experiment. The transition mid-point was found to be 24.7 T, with a width of 1.3 T, as reported in Fig. 13. The broken curve through this high-field point and the data near 7 T is a fit using the spin–orbit parameter, $\lambda_{SO} = 3.5$ and α (Maki parameter) = 1.35, but requiring a T_c which is 0.5 K lower than that actually observed. In the light of the preceding

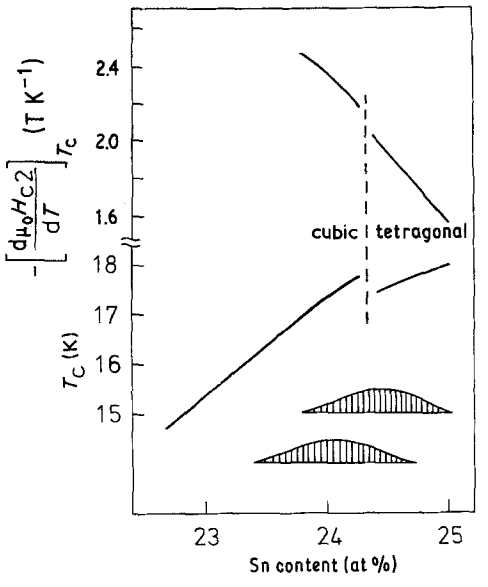

Figure 12 T_c near cubic–tetragonal phase boundary explaining the positive curvature of $H_{c2}(T)$. Insert: best-estimated concentration profiles.

remarks, these critical fields and the extrapolated value $H_{c2}(0) = 27.5$ T have to be attributed to under-stoichiometric cubic material shunting the tetragonal volume fraction.

4. Conclusion

In the present study, work was concentrated on the preparation of bulk A15-type Nb–Sn alloys covering the whole homogeneity range. The region of stability of the low-temperature tetragonal phase has been shown to be very narrow, extending to about 0.5 at % below the stoichiometric composition. The measurement of the relevant parameters of well-characterized specimens has enabled us to assess the important physical properties of this system. To our knowledge, the experiments discribed allowed for the first time a reliable comparison between measured and calculated critical field slopes throughout the homogeneity range of an A15-phase. It is concluded from the satisfactory agreement that the theory relating the critical field slopes to observable alloy parameters is basically correct.

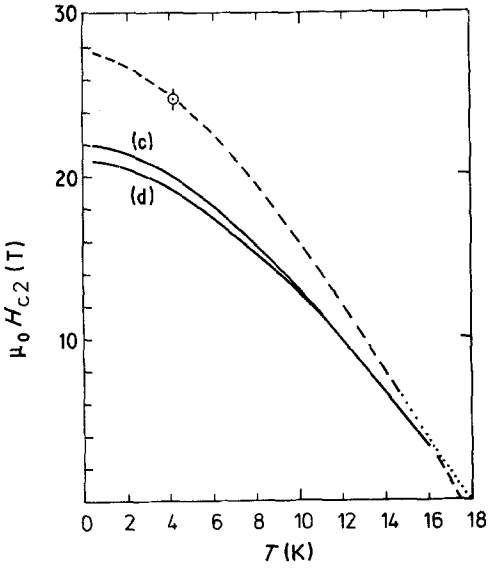

Figure 13 H_{c_2} of $Nb_{75.6}Sn_{24.4}$: static low-field transition: ·, pulsed field transition: o. Curves (c) and (d) represent isotropic theory in the clean and dirty limits, respectively, adjusted to $(\partial H_{c_2}/\partial T)_{T_c}$.

Acknowledgements

The authors wish to thank Messrs A. Naula, M. Cabrini and F. Liniger for their technical assistance, Professor Ø. Fischer for his discussions and Professor J. Bertrand for carrying out the microprobe analysis.

References

1. W. A. FIETZ, *IEEE Trans. Magn.* **Mag-15** (1979) 67.
2. J. MULLER, *Rep. Prog. Phys.* **43** (1980) 641.
3. L. J. VIELAND, *RCA Rev.* **25** (1964) 366.
4. V. N. SVECHNIKOV and V. M. PAN, *Sov. Phys. Doklady* **11** (1966) 152.
5. J. J. HANAK, K. STRATER and G. W. CULLEN, *RCA Rev.* **25** (1964) 342.
6. H. J. BODE and Y. UZEL, *Phys. Lett.* **24A** (1967) 141.
7. D. F. MOORE, R. B. ZUBECK, J. M. ROWELL and M. R. BEASLEY, *Phys. Rev. B* **20** (1979) 2721.
8. H. DEVANTAY, J. L. JORDA, R. FLÜKIGER and J. MULLER, unpublished work.
9. R. MAILFERT, B. W. BATTERMAN and J. J. HANAK, *Phys. Lett.* **24A** (1967) 315.
10. L. J. VIELAND, R. W. COHEN and R. REHWALD, *Phys. Rev. Lett.* **26** (1971) 373.
11. H. W. KING, F. H. COCKS and J. T. A. POLLOCK, *Phys. Lett.* **26A** (1967) 77.
12. L. J. VIELAND, *J. Phys. Chem. Sol.* **31** (1970) 1449.
13. R. FLÜKIGER, KFK Bericht 3140, Kernforschungszentrum, Karlsruhe, October, 1980.
14. R. HECHT, *RCA Rev.* **25** (1964) 453.
15. K. HECHLER, G. HORN, G. OTTO and E. SAUR, *J. Low Temp. Phys.* **1** (1969) 29.
16. D. M. KROEGER, D. S. EASTON, A. DasGUPTA, C. C. KOCH and J. O. SCARBROUGH, *J. Appl. Phys.* **51** (1980) 2184.
17. S. FONER and E. J. McNIFF, *Phys. Lett.* **58A** (1976) 318.
18. R. AKIHAMA, K. YASUKOCHI and T.

OGASAWARA, *IEEE Trans. Magn.* **MAG-13** (1977) 803.
19. T. P. ORLANDO, E. J. McNIFF, J. S. FONER and M. R. BEASLEY, *Phys. Rev. B* **19** (1979) 4545.
20. J. W. COLBY and S. F. NIEDERMEYER, US Atomic Energy Commission Report number NCLO-914 (1964).
21. J. L. JORDA, R. FLÜKIGER and J. MULLER, *J. Mater. Sci.* **13** (1978) 2471.
22. J. L. CHARLESWORTH, I. MACPHAIL and P. E. MADSEN, *ibid.* **5** (1970) 580.
23. P. FESCHOTTE, A. POLIKAR and G. BURRI, *C.R. Acad. Sc. Serie C* **288** (1979) 125.
24. R. FLÜKIGER and J. L. JORDA, *Sol. State Comm.* **22** (1977) 109.
25. A. JUNOD, J. MULLER, H. RIETSCHEL and E. SCHNEIDER, *J. Phys. Chem. Sol.* **39** (1978) 317.
26. S. J. WILLIAMSON, *Phys. Rev.* **B2** (1977) 3545.
27. J. A. WOOLLAM, R. B. SOMOANO and P. O'CONNOR, *Phys. Rev. Lett.* **32** (1974) 712.
28. P. ENTEL and M. PETER, *J. Low Temp. Phys.* **22** (1976) 613.
29. W. H. BUTLER, *Phys. Rev. Lett.* **44** (1980) 1516.

Received 9 December 1980 and accepted 13 January 1981.